PHOTOELASTICITY OF YVO4 THROUGH FIRST-PRINCIPLES CALCULATION

Amin Mirzai[1], Aylin Ahadi[1] & Solveig Melin[1]

[1] Department of Mechanical Engineering, Division of Mechanics
Lund University, Lund, Sweden
e-mail: amin.mirzai@mek.lth.se

Key words: Density Functional Theory (DFT), Tetragonal, Photoelastic Constants, Refractive Index, Optical Path Difference

Abstract. The laser host materials undergo relatively small changes in their intrinsic properties due to various sources during an experiment. These sources are often related to temperature change and vibrations due to crystal mounting, which may cause stress-induced birefringence in laser host materials[1]. Birefringence is a phenomenon that causes optical anisotropy due to external load or residual stress. As a result, the final outcome of the experiments can be affected. One way to reduce probable noises is to predict the change in optical properties with respect to load. In the case of laser host materials, refractive index is one of the most prominent properties that undergoes change. The change in refractive index due to external load in the linear response regime is known as photoelasticity. Therefore, to predict the change pattern of refractive index in a crystal, one needs to know the elastic and photoelastic constants of the material. Here, we extract the photoelastic tensor of YVO_4 crystal through application of density functional theory (DFT). This is important due to application of this crystal as a laser host and phosphor[2, 3].

1 INTRODUCTION

The YVO_4 is commonly used as a laser host and phosphor materials, and it is often doped with Lanthanide ions. Application of YVO_4 is mainly dependent on the optical properties of it. Therefore, one should be aware of its change due to external load on the crystal. One source of this external load is mechanical load due to mounting and change of the cavity due to probable temperature and pressure changes. This would change the length of the cavity and the optical path difference (OPD). The optical path difference is essentially the change in refractive index, n, along thickness of the crystal, d:

$$OPD = \Gamma = d\Delta n \tag{1}$$

So, here we propose that this change is traceable using intrinsic properties of the material, namely, elastic and photoelastic properties. The elastic properties would be helpful to see the change in physical length of the crystal under study, while photoelasticity is useful to trace the change in refractive index of the laser medium. Hence, in this study we extract the elastic and photoelastic tensors so that it could be utilized for a future FEM simulation to visualize optical path difference and shape deformation of the laser medium.

The basic idea behind the photoelastic effect is described in Equation 2. In this equation, e_{kl} is the strain tensor and p_{ijkl} is the photoelastic tensor coefficient.

$$\Delta B_{ij} = p_{ijkl}e_{kl} \tag{2}$$

Besides, in the above equation, ΔB is the difference between the inverse dielectric tensor of the strained and the unstrained equilibrium configuration. Both the inverse of dielectric tensor and the pure strain tensor e_{kl} are symmetrical 6×6 matrices. Therefore, p_{ijkl} will have 36 elements, out of which 21 generally will be independent elements due to following allowed permutations among its indices: (i↔j), (k↔l), and (ij↔kl). Moreover, due to tetragonal group symmetry of our crystal, the number of independent elements gets reduced to a total of 7[5]. The final representation of the photoelastic tensor for the I4$_1$/amd space group, is as follows.

$$p_{ijkl} = \begin{pmatrix} p_{11} & p_{12} & p_{13} & 0 & 0 & 0 \\ p_{12} & p_{11} & p_{13} & 0 & 0 & 0 \\ p_{31} & p_{31} & p_{33} & 0 & 0 & 0 \\ 0 & 0 & 0 & p_{44} & 0 & 0 \\ 0 & 0 & 0 & 0 & p_{44} & 0 \\ 0 & 0 & 0 & 0 & 0 & p_{66} \end{pmatrix} \tag{3}$$

The Equation 3 shows the photoelastic tensor, and its corresponding elements that can be obtained using Equation 4.

$$p_{ijkl} = \frac{\delta \Delta B_{ij}}{\delta e_{kl}} \tag{4}$$

This means that for each independent strain e_{kl}, listed in the appendix, the dielectric tensor is computed in such a way that photoelastic constants can be obtained by finite difference[9]. The full description of the computational scheme is explained in the next section.

1.1 Computational technique & method

The calculations of photoelastic tensors are carried out using the CRYSTAL code[7]. The crystal code uses linear combinations of Gaussian Type Functions (GTF) as basis sets to construct the fictitious wave functions. The exchange and correlation part of Hamiltonian were treated based on PBE0[8] and PBESOL0[10] methods. These hybrid functionals were specifically chosen to overcome the shortcoming of the semi-local functionals. An effective core potential atom-centered GTF basis sets of triple-ζ valence quality, augmented by a polarization function (TZVP), are adopted for each element in the system. The truncation criteria for bi-electronic integrals is controlled by five thresholds, which are set to 8, 8, 8, 10, 20. Last but not least, the sampling of the reciprocal space was conducted using a shrinking factor of 4, and the convergence criterion on total energy was set to 10^{-8} Hartree.

The overall flow of the photoelastic tensor extraction is depicted in the Figure 1. As the figure shows, at the first step the provided geometry is fully optimized, i.e. both cell and atomic positions are optimized with tight tolerance. Then a static self-consistence filed (SCF) calculation is performed on the optimized structure to get the total energy of the given structure. For the next step the ground state dielectric tensor of the system known as $\epsilon(0)$ is computed.
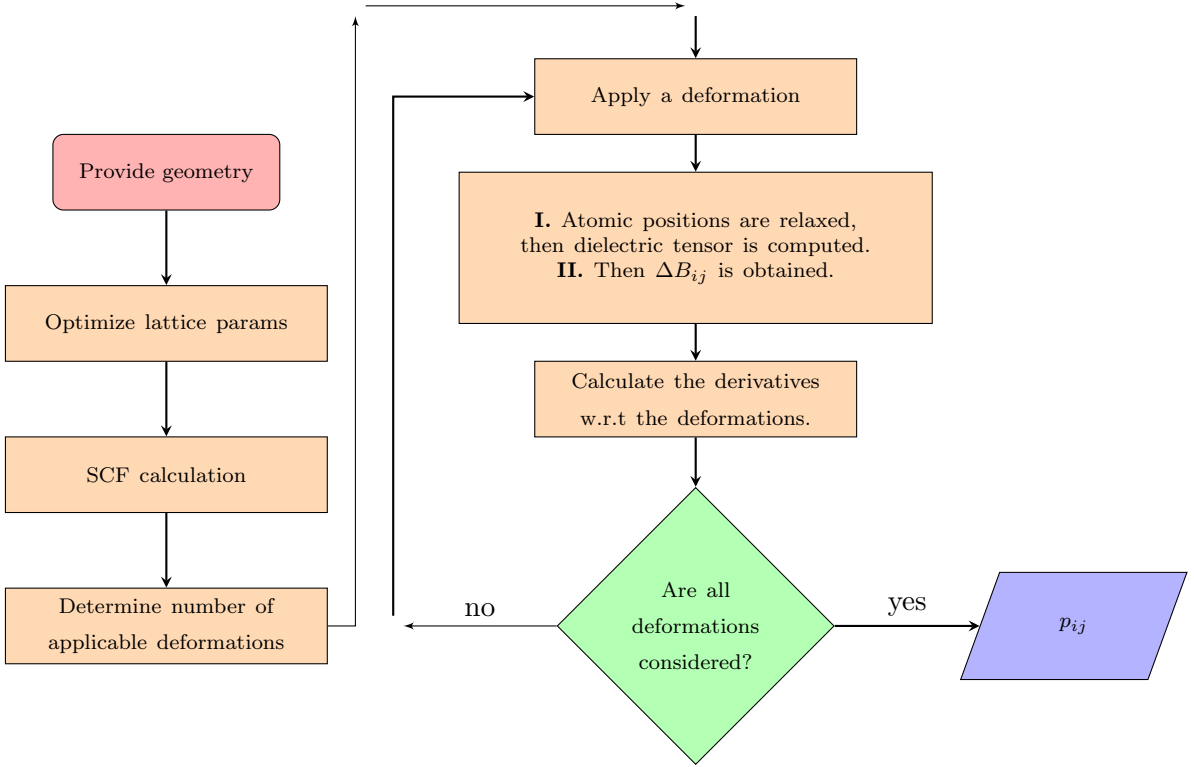
Figure 1: Workflow of photoelastic tensor extraction

This is done to produce a reference value for comparison. Later, one has to find out the necessary number of deformations for the corresponding geometrical system. Since the system under study in this paper has a Tetragonal symmetry, there are four pairs of strain deformations to be applied on the optimized geometry. These four strain matrices are presented in the appendix.

Once the geometry is deformed, the dielectric tensor of the deformed geometry is computed, and this step repeats until all allowed deformation are done. Then the difference between corresponding inverse dielectric tensor with respect to reference inverse dielectric tensor is computed. Essentially, a linear fit of ΔB_{ij} to strain, e. Finally, one can obtain the elements of the photoelastic tensor using Equation 4.

$$\Delta B_{ij} = [\epsilon^{-1}(e_{kl})]_{ij} - [\epsilon^{-1}(0)]_{ij} \tag{5}$$

2   Results & Discussion

Table 1 exhibits the photoelastic tensor of the YVO_4. The first row is dedicated to PBE0, and the second row is dedicated to PBESOL0 results. The photoelastic tensor, as discussed earlier, has 7 non-zero and unique elements. As seen the maximum value belongs to p_{31}, which is much larger compared to the rest of elements. This is true for both XC functionals, although there is a difference of 4 units between these two. In search of the reason for this large value, a modified version of the PBE0, which is known as PBE0-1/3[4] is employed for comparison. In

this functional the contribution of exact exchange has increased to 33 percent as opposed to 25 percent in normal PBE0. As you can see in the third row of Table 1, the value of p_{31} is reduced and it is now comparable to other non-zero elements in the tensor. The difference in magnitude of the p_{44} element between PBESOL0 and PBE0-1/3 has reduced as well, although the sign still remains an ambiguity. On the other hand, the determination of the sign of an element is known to be difficult even with experimental techniques such as interferometry and conoscopic. Hence, it is difficult to judge which sign is the correct one. Essentially, the inconsistency in sign of photoelastic tensor's elements can be referred to the finite wavelength of the laser sources in the experimental studies[9]. In any case the application of PBE0-1/3 has not only improved the agreement among the elements of the photoelastic tensor within the same row but also with the elements calculated by PBESOL0 XC functional.

Overall the validation of the calculated constants is difficult since to the best of our knowledge this is the first time one extracts the photoelastic constants of YVO_4, both experimentally and theoretically. However, the agreement between most of the elements is well, and the fact that increase in percentage of exact exchange improved the values of two ambiguous elements proves that the discrepancies are due to fundamental shortages of DFT and not a numerical error. Nevertheless, it may help to improve the validity of our calculated results by comparing those parameters that experimental or theoretical data are already available for them. Thus, we are comparing the elastic constants in Table 2, and dielectric values in Table 4.

Table 1: Photoelastic (elasto-optic) constants, p_{ij}.

	p_{11}	p_{12}	p_{13}	p_{31}	p_{33}	p_{44}	p_{66}
PBE0	0.191	0.146	0.078	9.525	0.033	-0.010	-0.077
PBESOL0	0.199	0.146	0.072	5.507	0.034	0.033	-0.078
PBE0-1/3	0.199	0.153	0.079	0.080	0.034	-0.018	-0.078

The elastic constants of the YVO_4 are calculated using both CRYSTAL and VASP[12] codes. Again, this is done to improve the validity of the results. As Table 2 exhibits, the results obtained by CRYSTAL are slightly higher. This can be seen specifically in C_{11} and C_{33}; in addition, the mean squared error (MSE) of these two elements are large values as well. It should be mentioned that the values of MSE are calculated for all rows of the tables that are obtained during this work. The discrepancy is mainly due to the difference between VASP and CRYSTAL, as VASP uses plane-waves for basis sets while CRYSTAL uses GTFs. This can be inferred by comparing the results between the pairs calculated by the same code. Nevertheless, the remaining four elements have a much smaller value of MSE that could be interpreted as high numerical accuracy. The point that should be emphasized here is that the discrepancies in C_{11} and C_{33} are not numerical errors but in fact related to the formulation of the corresponding code. To address this issue, we look at the equivalent values of these two elements in the photoelastic tensor, p_{11} and p_{33}, which are exceptionally close to each other. Since these elements of elastic and photoelastic tensors get extracted using the same deformation matrices, if there were any numerical errors both the elastic and the photoelastic tensors would have been affected. Hence, the large differences in the aforementioned elements of the elastic tensor solely stems from the difference in formulation of

the codes. Moreover, we have tabulated the variations of main elastic moduli in Table 3. Not

Table 2: Elastic constant of zircon-type YVO_4, VASP:*, CRYSTAL:ζ. All values are in GPa.

Type	C_{11}	C_{33}	C_{44}	C_{66}	C_{12}	C_{13}
AM05*	234.10	307.82	15.79	44.54	45.25	83.25
HSE06*	231.27	301.98	15.71	45.19	44.89	81.91
PBE0$^\zeta$	249.22	314.10	17.47	51.51	47.64	83.91
PBESOL0$^\zeta$	250.96	323.03	16.88	49.88	46.30	83.59
PBE0-1/3$^\zeta$	258.66	333.07	17.81	52.59	46.54	85.37
MSE	109.42	121.58	0.73	10.81	0.96	1.24
GGA[11]	216.10	284.80	21.90	45.50	44.30	78.80

to mention, the corresponding figures for the elastic moduli can be found in the appendix.

Table 3: Variation of the elastic moduli

	E_{min}(GPa)	E_{max}(GPa)	G_{min}(GPa)	G_{max} (GPa)	ν_{min}	ν_{max}
PBE0	61.39	266.67	17.476	96.766	0.0376	0.7571
PBESOL0	59.60	276.01	16.88	99.28	0.04	0.76
PBE0-1/3	62.69	285.3	17.81	102.71	0.03	0.76

To address the optical properties, we have also extracted the dielectric constants of the principle axes to compare and evaluate the accuracy as demonstrated in Table 4. The overall accuracy of the all calculated rows are in good agreement with each other. This can be deduced from MSE values as they are presented in the table. Furthermore, the deviation between the hybrid functionals PBE0, PBESOL0, PBE0-1/3 and the experimental values are: 7.93%, 7.52%, and 11.02% for $\epsilon_x = \epsilon_y$, and 9.33%, 8.61%, and 12.74% for ϵ_z, respectively.

Table 4: Principal axis components of static dielectric tensor.
VASP:*, CRYSTAL:ζ

YVO_4	$\epsilon_x = \epsilon_y$	ϵ_z
AM05*	3.983	4.864
HSE06*	3.976	4.734
PBE0$^\zeta$	3.481	4.185
PBESOL0$^\zeta$	3.497	4.218
PBE0-1/3$^\zeta$	3.365	4.028
MSE	0.069	0.108
Exp.(15°C[13])	3.7818	4.6164

3 Conclusion & future work

We have extracted the photoelastic (elasto-optic) constants of YVO_4 using GTF based CRYSTAL code. To the best of our knowledge, this is the first time one extracts the photoelastic tensor of the YVO_4 both theoretically and experimentally. For this reason the validation of extracted constants remains an issue that should be addressed either with experimental measurements or more theoretical calculations. Furthermore, it might be possible to validate current data with experiments other than techniques that deal with extraction of the photoelastic tensor. The current data can be utilized in a FEM simulation to identify the linear change in refractive index of the laser medium. Later, the identified variation of OPD can be used to tune and to designate the right orientation of the beam light for experiments such as laser stabilization. This would allow the beam light to lock on the right resonance frequency. An improvement in the outcome of the experiment can be interpreted as validation of the calculated photoelastic tensor and vice versa. This way it might be possible to circumvent the cumbersome acousto-optic experiments for determination of the photoelastic tensor.

4 Acknowledgements

REFERENCES

[1] Ostermeyer, M., Mudge, D., Veitch, P. & Munch, J. Thermally induced birefringence in Nd:YAG slab lasers. *Appl. Opt.*. **45**, 5368-5376 (2006,7), http://www.osapublishing.org/ao/abstract.cfm?URI=ao-45-21-5368

[2] Fields, R., Birnbaum, M. & Fincher, C. Highly efficient Nd : YVO_4 diode-laser end-pumped laser. *Applied Physics Letters*. **51**, 1885-1886 (1987),

[3] Li, Y., Zheng, Y., Wang, Q. & Zhang, C. Synthesis of luminescent YVO_4 : Eu^3+ submicrometer crystals through hydrogels as directing agents. *Materials Chemistry And Physics*. **135**, 451-456 (2012), https://www.sciencedirect.com/science/article/pii/S0254058412004543

[4] Guido, C., Brémond, E., Adamo, C. & Cortona, P. Communication: One third: A new recipe for the PBE0 paradigm. *The Journal Of Chemical Physics*. **138**, 021104 (2013)

[5] Narasimhamurty, T. Photoelastic and Electro-Optic Properties of Crystals. (Springer)

[6] Powell, R. Symmetry, group theory, and the physical properties of crystals. (Springer,2010)

[7] Dovesi, R., Erba, A., Orlando, R., Zicovich-Wilson, C., Civalleri, B., Maschio, L., Rérat, M., Casassa, S., Baima, J., Salustro, S. & Others Quantum-mechanical condensed matter simulations with CRYSTAL. *Wiley Interdisciplinary Reviews: Computational Molecular Science*. **8**, e1360 (2018)

[8] Adamo, C. & Barone, V. Toward reliable density functional methods without adjustable parameters: The PBE0 model. *The Journal Of Chemical Physics*. **110**, 6158-6170 (1999)

[9] Erba, A. & Dovesi, R. Photoelasticity of crystals from theoretical simulations. *Phys. Rev. B.* **88**, 045121 (2013,7), https://link.aps.org/doi/10.1103/PhysRevB.88.045121

[10] Perdew, J., Ruzsinszky, A., Csonka, G., Vydrov, O., Scuseria, G., Constantin, L., Zhou, X. & Burke, K. Restoring the Density-Gradient Expansion for Exchange in Solids and Surfaces. *Phys. Rev. Lett.*. **100**, 136406 (2008,4), https://link.aps.org/doi/10.1103/PhysRevLett.100.136406

[11] Huang, Z., Feng, J. & Pan, W. Theoretical investigations of the physical properties of zircon-type YVO4. *Journal Of Solid State Chemistry.* **185** pp. 42-48 (2012)

[12] Kresse, G. & Furthmüller, J. Efficiency of ab-initio total energy calculations for metals and semiconductors using a plane-wave basis set. *Computational Materials Science.* **6**, 15 - 50 (1996), http://www.sciencedirect.com/science/article/pii/0927025696000080

[13] Jacob, M., Mazierska, J. & Krupka, J. Dielectric properties of Yttrium Vanadate crystals from 15 K to 295 K. *Journal Of Electroceramics.* **15**, 237-241 (2005)

Appendix

$$e_1 = \begin{pmatrix} \delta & 0 & 0 \\ 0 & 0 & 0 \\ 0 & 0 & 0 \end{pmatrix} \qquad e_3 = \begin{pmatrix} 0 & \delta & 0 \\ \delta & 0 & 0 \\ 0 & 0 & 0 \end{pmatrix}$$

$$e_2 = \begin{pmatrix} 0 & 0 & 0 \\ 0 & 0 & 0 \\ 0 & 0 & \delta \end{pmatrix} \qquad e_4 = \begin{pmatrix} 0 & 0 & 0 \\ 0 & 0 & \delta \\ 0 & \delta & 0 \end{pmatrix}$$

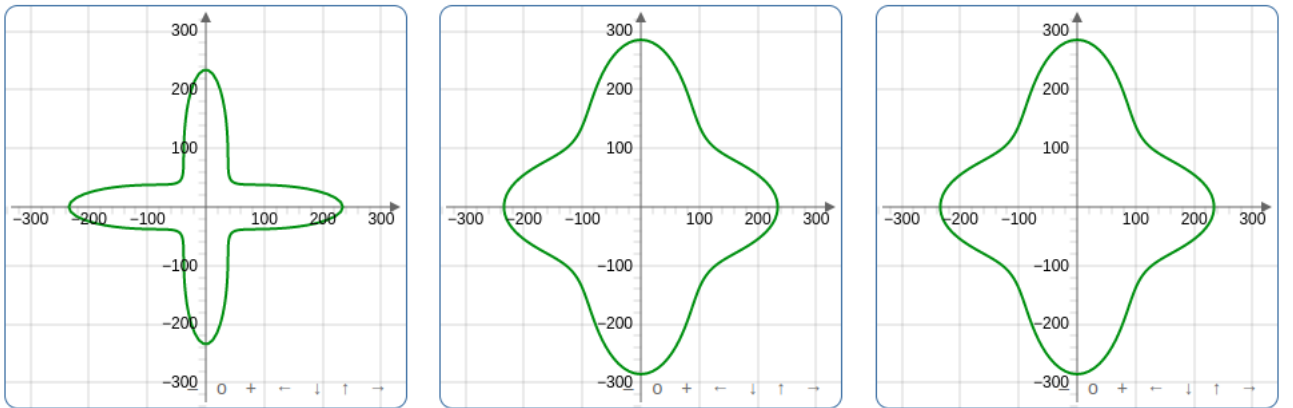

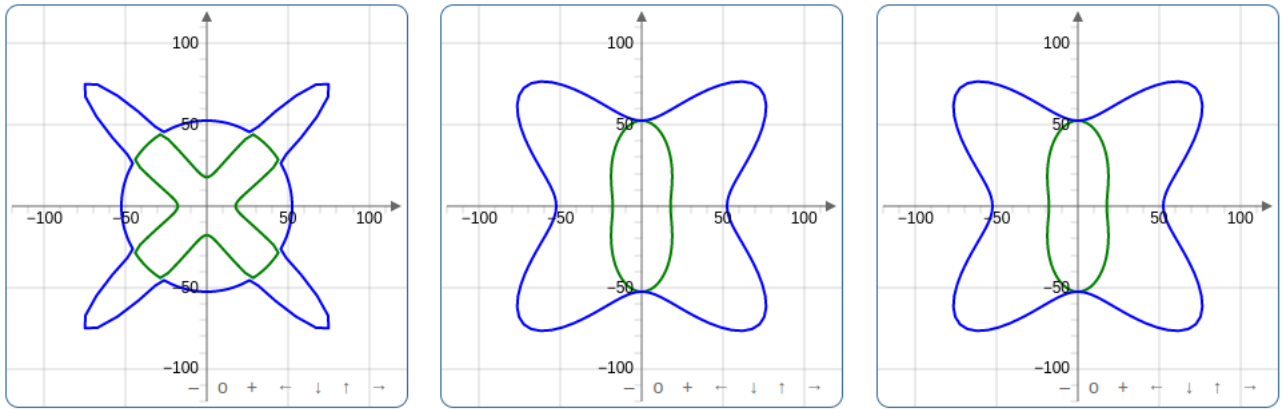Figure 2: Young modulus representation calculated by PBE0-1/3 in *xy*, *xz*, and *yz* planes, respectively.

Figure 3: Shear modulus representation calculated by PBE0-1/3 in xy, xz, and yz planes, respectively.
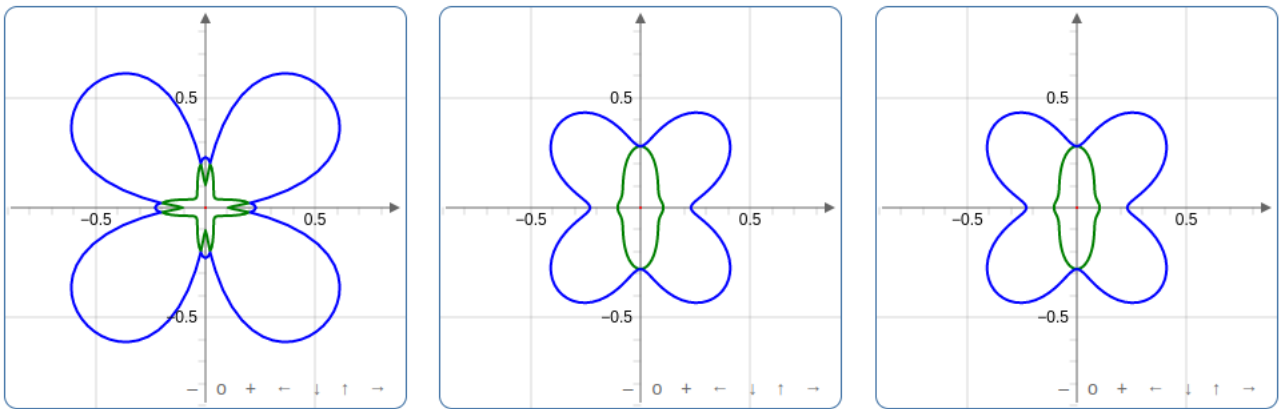

Figure 4: Poisson's ratio representation calculated by PBE0-1/3 in xy, xz, and yz planes, respectively.